Flea-Inspired Catapult Mechanism for Miniature Jumping Robots

Minkyun Noh, Seung-Won Kim, *Student Member, IEEE*, Sungmin An, Je-Sung Koh, *Student Member, IEEE*, and Kyu-Jin Cho, *Member, IEEE*

***Abstract*—Fleas can jump more than 200 times their body length. They do so by employing a unique catapult mechanism: storing a large amount of elastic energy and releasing it quickly by torque reversal triggering. This paper presents a flea-inspired catapult mechanism for miniature jumping robots. A robotic design was created to realize the mechanism for the biological catapult with shape memory alloy (SMA) spring actuators and a smart composite microstructure. SMA spring actuators replace conventional actuators, transmissions, and the elastic element to reduce the size. The body uses a four-bar mechanism that simulates a flea's leg kinematics with reduced degrees of freedom. Dynamic modeling was derived, and theoretical jumping was simulated to optimize the leg design for increased takeoff speed. A robotic prototype was fabricated with 1.1-g weight and 2-cm body size that can jump a distance of up to 30 times its body size.**

***Index Terms*—Biologically inspired robot, biomimetics, catapult mechanism, flea robot, jumping robot, microrobot, smart composite microstructure (SCM), shape memory alloy (SMA) spring.**

I. Introduction

THE miniaturization of mobile robots inherently reduces their mass, which leads to low power consumption, low manufacturing cost, and agility. Miniature mobile robots with these characteristics are suitable for reconnaissance or sensing missions. Furthermore, miniature mobile robots allow a range of strategies when combined with larger scale carrier robots.

However, as robots get smaller, overcoming large obstacles and distances presents challenges due to their limited stride and body size. In biology, this effect is referred to as the "size grain hypothesis" [1]. Nature is full of examples of small animals and insects that can overcome this effect and travel large distances quickly. In order to increase the chances of survival, small creatures have developed various types of locomotion, such as jumping or flying, to rapidly escape danger. Inspired by nature, various small robots have been developed.

For aerial locomotion, a microrobotic fly has been developed [2]. The robot simulates not only the flapping kinematics but also the anatomy of a fly's thorax, which helps us to effectively generate a lift force. For terrestrial locomotion, a variety of jumping robots have been developed so far [4]–[19]. These robots widely employ catapult mechanisms, which small creatures rely on to generate large speed at takeoff within a short stretching length of the leg [3].

The catapult mechanisms of existing jumping robots are mostly based on DC motors (see Table 1). The hopper [4] stores elastic energy in a linear spring via a lead screw and gear. Storing action continues until a microswitch is tripped, and an additional storing action unlocks a latch to release the spring. Mini-Whegs [5] employs a partially toothed pinion and a gear that is linked to a linear spring. As the pinion rotates the gear, the spring is gradually extended. When the gear is disengaged from the pinion and slips, the spring is quickly released. Jollbot [6] has a steel-wired outer shell that functions as elastic energy storage. The shell is linked to a semicircularly grooved face cam via slider roller. As the roller moves along the grooved path, the outer shell gradually flattens and quickly recovers the original round shape to generate a catapult motion. Grillo[1] [7] stores elastic energy in a linear spring via a spiral-shaped cam. As the cam rotates, the gradually increasing cam radius compresses the spring. When the cam rotates to the escapement position, the cam radius suddenly drops, and the spring is quickly released. Grillo[2] [8], [9] employs a partially toothed pinion and linear spring to build the catapult mechanism, which is similar to that in Mini-Whegs. A miniature 7-g jumping robot [10]–[12] uses a torsional spring as energy storage. In order to gradually load and quickly release the spring, the robot employs a spiral-shaped cam and additional gears, similar to Grillo[1]. Closed elastica [13], [14] uses snap-through buckling of an elastic strip. The two ends of an elastic strip are fixed to rotational joints. As one of the joints rotates, the strip gradually deforms and suddenly buckles to generate the catapult motion. Basically, catapult mechanisms based on DC motors require additional mechanical elements to amplify motor torque and build up the power train, which presents challenges to miniaturized systems [15].

There have been attempts to develop catapult mechanisms for small jumping robots by using nonconventional actuators (see Table I). Microbot [16] employs a dielectric elastomer actuator (DEA). A DEA pumps mechanical energy into a spring over one or more actuation cycles via a ratcheting transmission.

Manuscript received December 8, 2011; revised April 6, 2012; accepted April 28, 2012. Date of publication May 25, 2012; date of current version September 28, 2012. This paper was recommended for publication by Associate Editor Y. Sun and Editor B. J. Nelson upon evaluation of the reviewers' comments. This work was supported by the Research Center Programs through the National Research Foundation of Korea funded by the Ministry of Education, Science and Technology under Grant 2009-0082824, Grant 2009-0070058, and Grant 2009-0087640.

The authors are with the Biorobotics Laboratory, School of Mechanical and Aerospace Engineering, Institute of Advanced Machinery and Design, Seoul National University, Seoul 151-742, Korea (e-mail: nomk1311@snu.ac.kr; demian05@snu.ac.kr; sman@snu.ac.kr; kjs15@snu.ac.kr; kjcho@snu.ac.kr).

This paper has supplementary downloadable material available at http://ieeexplore.ieee.org. This includes one multimedia MP4 format movie clip, which shows the jumping performance of the robot. This material is 4.6 MB in size.

Color versions of one or more of the figures in this paper are available online at http://ieeexplore.ieee.org.

Digital Object Identifier 10.1109/TRO.2012.2198510

TABLE I
CATAPULT MECHANISMS FOR SMALL JUMPING ROBOTS

Robot	Actuator	Energy Storage	Storing Mechanism	Releasing Mechanism
Hopper	DC motor	Linear spring	Lead screw and gear	Additional storing releases the latch
Mini-Whegs	DC motor	Linear spring	Partially toothed pinion and gear	Escapement mechanism
Jollbot	DC motor	Steel-wire	Face cam and slider roller	Escapement mechanism
Grillo[1]	DC motor	Linear spring	Lead screw, gear, and spiral cam	Escapement mechanism
Grillo[2]	DC motor	Linear spring	Partially tooted pinion and gear	Escapement mechanism
7g Robot	DC motor	Torsional spring	Spiral cam and gear	Escapement mechanism
Closed Elastica	DC motor	Elastic strip	Motor bends elastic strip	Snap-through buckling
Micro Explorer	DEA	Leaf spring	Ratcheting transmission	Passive release
Jumping Microbot[1]	Inchworm motor	Silicon rubber	Inchworm motor deforms rubber	Electrostatic trigger
Jumping Microbot[2]	Propulsion	Compound	Chemical	Ignition
Voice Coil Hopper	Voice coil	Capacitor	Capacitor is charged with electrical energy	Electromagnetic coupling
Flea-inspired Robot	SMA spring	SMA spring	Phase transition of SMA spring	Trigger muscle reverses latching torque

When the level of energy stored in the spring crosses a predefined threshold, the energy is released to provide hopping power. Voice Coil Hopper [15] uses a voice coil actuator, whose operating principle is based on electromagnetic coupling. Jumping Microbot[1] [17], [18] uses an electrostatic inchworm motor and silicone microrubber bands. It also has an electrostatic trigger system. Jumping Microbot[2] [19] uses chemical propulsion to jump.

This paper presents a flea-inspired catapult mechanism for miniature jumping robots. Fleas jump by employing a unique catapult mechanism: storing a large amount of elastic energy and releasing it quickly by torque reversal triggering. To store energy, a main muscle compresses an elastic element known as resilin. A small triggering muscle unlocks a structural latch, thereby releasing the energy [20]. From a mechanical point of view, the torque reversal triggering is attractive since it can handle large elastic energy easily. An attempt was made to take advantage of the flea's mechanism with shape memory alloy (SMA) spring actuators. SMA actuators help simplify the mechanism by serving two functions: those of the biological muscle and the resilin pad in a flea. Phase transition by electrical heating enables SMA springs to store more energy without additional displacement. In addition, SMA spring actuators enable the system to discard additional mechanical elements; thus, our mechanism is scalable.

A robotic design based on this mechanism was proposed (see Fig. 1). A four-bar mechanism was used to simulate the kinematics of a jumping insect's leg with reduced degrees of freedom [8]. Dynamic modeling was derived and theoretical jumping was simulated to optimize the leg design so as to increase the speed at takeoff. A robotic prototype (Fig. 1) was fabricated with the smart composite microstructure (SCM) [21], [31] process. The prototype weighs 1.1 g, is 2 cm long, and can jump a distance of up to 30 times its body size. The jumping height can be adjusted by varying the amount of current input. The prototype is tethered to an external power supply unit through enameled wire.

The proposed catapult mechanism inspired by a flea's leg is advantageous for handling large elastic energy due to the torque reversal triggering. In addition, SMA spring actuators enable the mechanism to be simple and scalable. This new mechanism has a potential to further miniaturize the jumping robots.

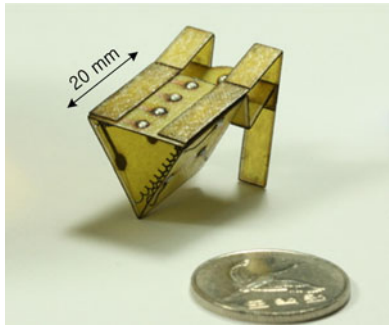

Fig. 1. Robotic prototype based on a flea-inspired catapult mechanism for miniature jumping robots. The diameter of the coin is 26.5 mm.

II. BIOINSPIRATION FROM FLEA JUMPING

A tiny flea can jump more than 200 times its body length [22]; it can serve as a model for miniaturized jumping robots. Fleas generate sufficient speed at takeoff via a catapult mechanism that gradually stores elastic energy and releases it quickly. Two catapult types have been proposed to explain the flea's jump. The Rothschild model [23]–[25] hypothesizes that the recoil of the spring pushes the trochanter (knee) onto the ground, thereby generating the jump. This model has dynamics similar to that of a mass–spring system. The Bennet–Clark model [20] proposes that the recoil of the spring acts through a lever system to push the tibia (shin) and tarsus (toe) onto the ground. Recently, Sutton and Burrows have published a research article with results that strongly corroborated the Bennet–Clark model [26].

A. Mechanism of a Flea's Catapult

A flea's catapult consists of muscles, cuticles, and an elastic element known as resilin (see Fig. 2). Basically, a flea extends its femur with the extensor muscle and flexes it with the flexor muscle. As the femur flexes [see Fig. 2(a)], the extensor muscle crosses the rotational joint. Next, the extensor muscle contracts,

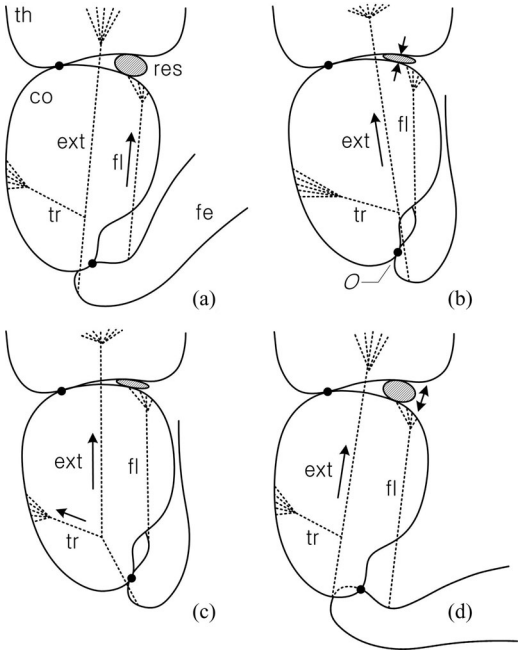

Fig. 2. Schematic of a flea's catapult. Three links are connected serially: th is the thorax, co is the coxa, and fe is the femur. A resilin pad (res) is located between the thorax and coxa, which function as a compression spring. Three muscles are arranged in the leg: fl is the flexor, ext is the extensor, and tr is the trigger muscle.

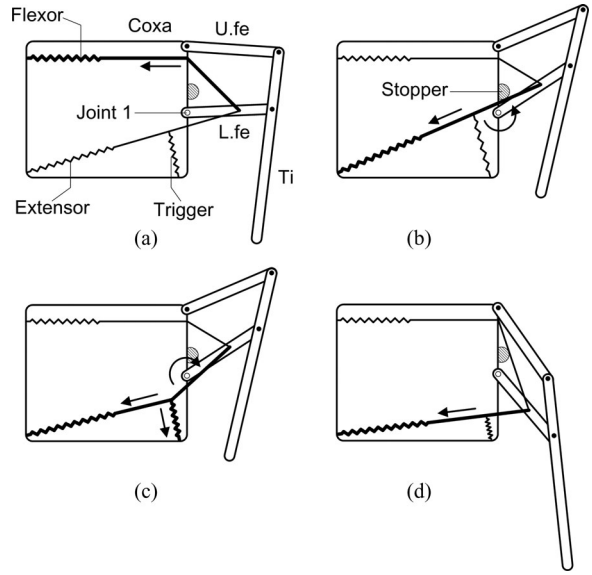

Fig. 3. Schematic design for miniature jumping robots based on a flea-inspired catapult mechanism. Three SMA springs function as artificial muscles: the extensor, trigger, and flexor. U.fe is the upper femur, and L.fe is the lower femur. Joint 1 was specially designed so that the extensor spring can pass through the rotational axis.

but the femur does not extend since it is in latch mode [see Fig. 2(b)]; the tensile force of the extensor muscle generates a torque in the direction of the flexing femur, thereby compressing the resilin pad and storing the elastic energy. When the trigger muscle pulls the extensor muscle across the rotational joint [see Fig. 2(c)], the line of extensor tensile force moves slightly, which leads to torque reversal; the latching torque is reversed to extending torque. Consequently, the catapult rapidly discharges the stored elastic energy and extends the leg [see Fig. 2(d)].

Although the flea's catapult mechanism uses three muscles to generate jumping motion, which might seem expensive for small creatures [3], it has some advantages from a mechanical point of view. First, it can securely store elastic energy; the entire cuticular exoskeleton of the coxa and femur function as a robust latch system that can withstand a relatively large spring force. In addition, the more the elastic energy stored, the firmer the latching. Second, it is easy to unlock the latch: The trigger muscle is attached almost perpendicularly to the extensor muscle, which provides a large mechanical advantage and avoids friction.

B. Flea-Inspired Catapult With Shape Memory Alloy Spring

Despite the limitations of hysteresis, large power consumption, and difficult handling and control, SMA spring actuators have properties advantageous for the development of microrobotic systems: 1) SMA springs have high power-mass density [27]; 2) SMA springs can be superposed to change the direction of the actuating force: The force direction of an SMA spring can be changed by directly attaching another SMA spring in a different direction; 3) SMA springs can be downscaled easily; and 4) SMA coil springs do not need additional mechanical elements for a transmission system since the spring itself functions as a transmission. The spring design reduces the force and increases the displacement of the SMA wire actuator [28].

A design for miniature jumping robots is proposed here to realize a flea-inspired catapult mechanism with SMA spring actuators. Three SMA actuators are arranged in the robot: the flexor, extensor, and trigger (see Fig. 3). The flexor and extensor are attached between the coxa and lower femur, which function as antagonistic actuators to each other. The trigger is attached to the extensor almost perpendicularly for efficient triggering. The joint between the coxa and lower femur, which is named Joint 1, was designed with an overcenter characteristic; it can pass the extensor spring through the rotational axis.

Assume that the robot has just finished jumping and that the leg needs to be flexed to prepare for the next jumping cycle [see Fig. 3(a)]. The sequence begins by activating the flexor with an electric current. The flexor contracts and folds the leg to a crunched position. The extensor is pulled and passes through Joint 1. Folding stops when the lower femur touches a stopper on the body [see Fig. 3(b)]. To initiate jumping, the extensor is activated with an electric current. Although the purpose of the extensor is to extend the legs, in this state, the extensor force will only generate torque in the folding direction. The stopper blocks the extensor from contracting and enables a large amount of energy to be stored in the extensor. Activation of the trigger attached to the extensor pulls the extensor past Joint 1 such that the force applied by the extensor generates a torque in the direction of leg extension [see Fig. 3(c)]. As the femur rotates, the moment arm increases, thereby generating a gradually increasing torque [see Fig. 3(d)].

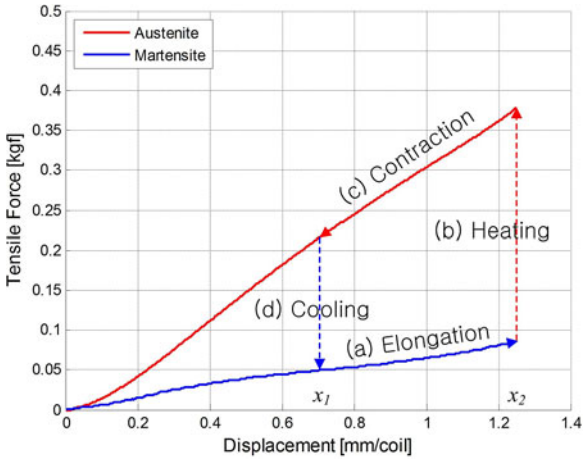

Fig. 4. Force–displacement cycle curve for a single coil of the extensor spring.

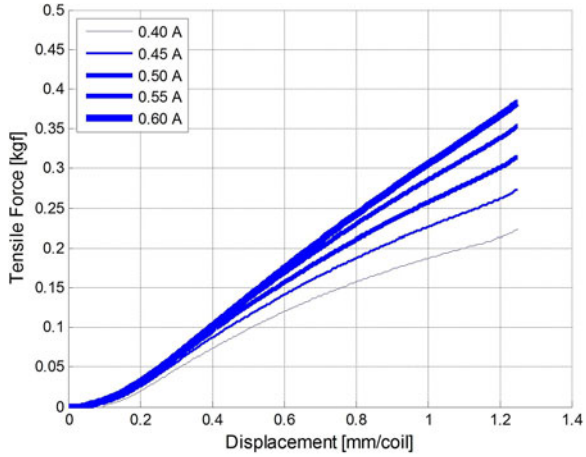

Fig. 5. Force–displacement curve for a single coil of the extensor spring with respect to various input currents. The stiffness increases proportionally to the amount of current input.

During the jump, the extensor spring undergoes a force–displacement cycle that consists of four stages: elongation, heating, contraction, and cooling (see Fig. 4). In the elongation stage (a), the extensor is lengthened and latched at displacement x_2. The external work input is relatively small because of the low stiffness of the martensite phase. In the heating stage (b), the extensor is heated by an electric current and undergoes phase transition to the austenite phase. During the phase transition, the extensor stores more elastic energy by increasing its stiffness. The force increases along the constant displacement line. In the contraction stage (c), the latch is released by triggering, and the extensor contracts to displacement x_1. During this stage, the catapult discharges the elastic energy stored. Finally, in the cooling stage (d), the electric current is cut and the spring is cooled. The force decreases along the constant displacement line, and the mechanism thus returns to the initial state.

Through the phase transition, the SMA spring stores elastic energy without any supplementary energy storage elements. This is quite different from the biological catapult in a flea. Since muscles have an inherent limit with regard to contraction speed, they should be accompanied with elastic elements, such as tendons and resilin pads, to enable jumping insects to generate fast action [3]. However, in this study, a single SMA spring serves the role of both the biological muscle and the resilin pad of a flea. In addition, an SMA spring can vary its stiffness according to the current input, thereby adjusting the amount of elastic energy stored without changing the displacement. Thanks to this characteristic, our mechanism can adjust the jumping height without any structural tuning and transmission system.

The force–displacement curves for a single coil were obtained from an actual tensile test on SMA springs (see Figs. 4 and 5). The test specimens were made of Flexinol actuator wire (70 °C as temperature and 0.254-mm diameter). The wire was coiled into a spring with a diameter of 1 mm; the spring was annealed at 300 °C for 1 h. Each specimen was trained by electrical heating before the experiment. First, the martensite curve was measured while increasing the spring displacement from zero to 1.25 mm/coil. Second, different amounts of electric current were applied to the specimen, and the SMA spring changed phase to austenite at a constant displacement of 1.25 mm/coil. Third, austenite curves were measured while decreasing the spring displacement from 1.25 mm/coil to zero. The results show that the stiffness of a single coil increases proportionally to the amount of current input (see Fig. 5). The maximum allowable current input was 0.6 A, above which the SMA spring began to degrade.

III. Robot Design

A. Body Design

A body was designed to realize the flea-inspired catapult mechanism with an SCM. A four-bar mechanism was used to simulate an insect's leg with reduced degrees of freedom. The body is comprised of three planar structures: one for the main body and two for the legs (see Fig. 6). The main body consists of five planar links: $B1$–$B5$. On folding, the planar structure becomes a 3-D catapult structure. Link $B1$ is named the lower femur, and the triangular structure, which consists of $B2$–$B5$, is named the coxa. The leg consists of three rigid links: $L1$–$L3$. $L2$ is named the upper femur, and $L3$ is the tibia. $L1$ is for adhesion to the main body. The coxa, upper femur, lower femur, and tibia comprise a closed four-bar system (see Fig. 7). As the lower femur rotates, the tibia moves according to the four-bar constraints and simulates a flea extending its leg. Concurrently, the extensor spring rotates toward the lower edge of the body. If a in Fig. 7 is too long, the extensor may touch the lower edge of the body. Therefore, a is limited to 6 mm.

As shown in Figs. 3 and 7, the stroke of the extensor spring (ΔX) is determined by the body design; one tip of the spring needs to be fixed to the coxa, and the other tip needs to be fixed to the lower femur. The stroke of the extensor spring is

$$\Delta X = X_2 - X_1 \tag{1}$$

where X_2 is the extensor displacement after elongation, and X_1 is the extensor displacement after contraction. X_2 is determined by the distance between the attachment points when the lower femur is in line with the extensor [see Fig. 3(b)], and X_1 is

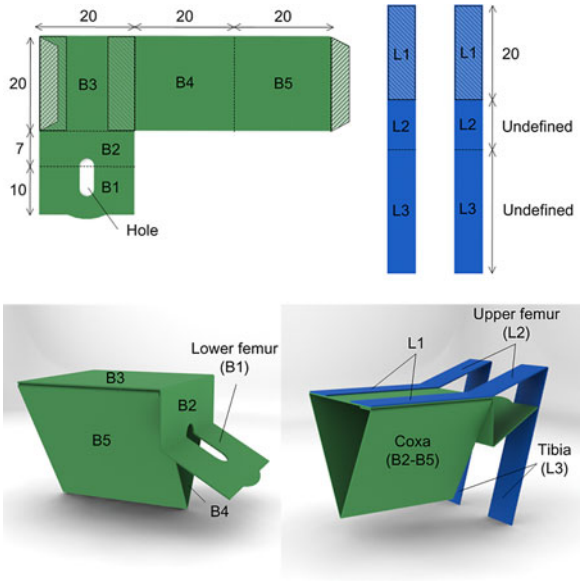

Fig. 6. Body design for miniature jumping robots based on a flea-inspired catapult mechanism. Planar structures become a 3-D structure when folded. Dashed regions are for adhesion.

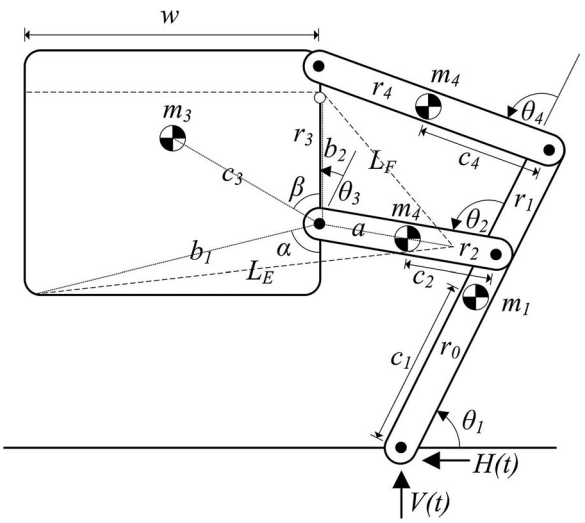

Fig. 7. Schematic of the robot. The robot uses a four-bar mechanism. L_E is the length of the extensor, and L_F is the length of the flexor.

determined by the distance between the attachment points when the leg is fully extended [see Fig. 3(d)].

B. Extensor Design

The extensor consists of a spring and tendon (see Fig. 8). The length of the extensor L_E is the sum of the spring initial length S_0, tendon length T_0, and spring displacement X

$$L_E = N(x + s_0) + T_0 \tag{2}$$

where N is the coil number, x is the spring displacement per coil (X/N), and s_0 is the spring initial length per coil (S_0/N). After the elongation is finished, or x reaches x_2 in Fig. 4, L_E becomes the sum of b_1 and a in Fig. 7 according to the body design.

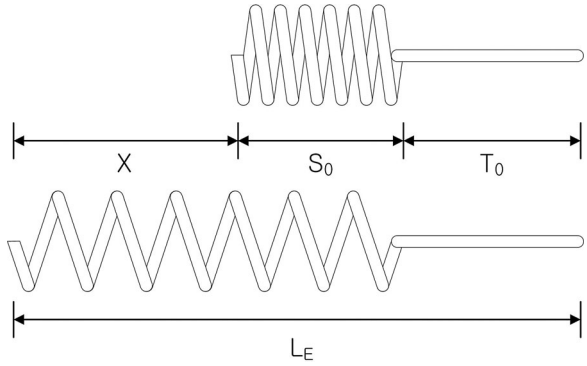

Fig. 8. Design of the extensor: L_E is the length of the extensor, which is the sum of the tendon length T_0, spring initial length S_0, and spring displacement X.

The goal of the extensor design is to maximize the elastic energy stored in the spring part. According to the experimental results, the extensor coil spring in the austenite phase can be modeled as a linear spring (see Fig. 5). Thus, elastic energy stored in the extensor coil spring is

$$E = G\frac{d^4}{16D^3N}(X_2^2 - X_1^2) \tag{3}$$

where G is the shear modulus of the full austenitic spring, d is the wire diameter, D is the spring diameter, and N is the number of coils in the spring. According to (1) and (2), (3) becomes

$$E = G\frac{d^4}{16D^3}\left(\left(2\Delta X - \frac{\Delta X^2}{a + b_1 - T_0}\right)x_2 - \frac{s_0\Delta X^2}{a + b_1 - T_0}\right). \tag{4}$$

To maximize the energy stored, the wire diameter d needs to be increased, the spring diameter D needs to be decreased, and the spring displacement per coil after elongation x_2 needs to be increased to the limit. We chose the thickest possible SMA wire (diameter of 0.254 mm) and coiled the wire into a spring whose diameter was 1 mm. According to the experimental result, the maximum allowable displacement to avoid yielding was 1.25 mm/coil ($x_{2,\max}$), and the initial spring length per coil was 0.6 mm/coil (s_0). Using (2), coil number N was calculated to be 11, for which the stiffness of the extensor spring is 300 N/m. Two extensor springs were installed in parallel to enhance the catapult power. Therefore, the net stiffness of the extensor was 600 N/m, which was used to establish a mathematical model for the robot.

The stored energy can also be measured from the tensile test of the SMA spring, which is shown in Fig. 4. The area under the contraction curve between x_1 and x_2 is the energy stored in the single coil of the extensor spring. To maximize the stored energy, the slope of the curve and x_2 need to be maximized. The maximum value of x_2 is determined by the yield limit, and the slope is determined by the wire and spring diameter. x_1 is the prestrain of the single coil of the extensor spring.

C. Flexor Design

The flexor spring functions as an antagonistic actuator to the extensor spring. To reduce the cooling time, we employed a

TABLE II
SPECIFICATIONS FOR THE SMA SPRING ACTUATORS

	Extensor	Trigger	Flexor
Wire Diameter (mm)	0.254	0.203	0.203
Core Diameter (mm)	1.000	0.560	0.560
Coil Number	11	15	50

wire thinner than that used for the extensor spring (diameter of 0.203 mm) and coiled the wire into a spring with a diameter of 0.56 mm.

The goal of the flexor spring design was to generate sufficient opposite torque to rotate the femur to the leg folding direction after each jump. At this stage [see Fig. 3(a)], the extensor spring is fully martensitic, and the flexor spring is fully austenitic. The stiffness of the fully martensitic extensor spring is about 30% that of fully austenitic extensor spring. The flexor spring should be designed to generate a torque larger than the torque generated by the fully martensitic extensor spring. Thus, the minimum required force of the flexor spring was about 0.2 kgf. Considering the additional friction force, we designed the flexor spring to generate up to 0.3 kgf by adjusting the coil number.

D. Trigger Design

The required force for the trigger is theoretically very small due to the large mechanical advantage [see Fig. 3(c)]. We employed the same wire and spring diameters as the flexor for manufacturing convenience. The coil number was selected considering the required displacement for triggering. The specifications for the SMA spring actuators are shown in Table II.

IV. MODELING AND OPTIMIZATION

A mathematical model was derived to predict and maximize the theoretical jumping speed of the robot. The coxa, upper femur, lower femur, and tibia were modeled as rigid bodies. Each flexure joint was modeled as a pin joint since the flexure length is sufficiently smaller than the link length [29]. The torsional stiffness of the flexure joint was neglected since the energy storable in the joint was significantly smaller than the energy stored by the extensor spring. With the assumption of no slip on the ground, the tip of the tibia was modeled as a pin joint until takeoff. Takeoff occurs when the vertical reaction force from the ground reaches zero.

A. Kinematics and Dynamics

The model of the robot consists of four rigid links, five rotational joints, and the ground (see Fig. 7). Four variables (θ_1, θ_2, θ_3, and θ_4) were introduced to describe the position and orientation of each link

$$\overrightarrow{P_1} = \begin{pmatrix} c_1 \cos\theta_1 \\ c_1 \sin\theta_1 \end{pmatrix} \tag{5}$$

$$\overrightarrow{P_2} = \begin{pmatrix} r_0 \cos\theta_1 + c_2 \cos(\theta_1 + \theta_2) \\ r_0 \sin\theta_1 + c_2 \sin(\theta_1 + \theta_2) \end{pmatrix} \tag{6}$$

$$\overrightarrow{P_3} = \begin{pmatrix} r_0 \cos\theta_1 + r_2 \cos(\theta_1 + \theta_2) + c_3 \cos(\theta_1 + \theta_3 + \beta) \\ r_0 \sin\theta_1 + r_2 \sin(\theta_1 + \theta_2) + c_3 \sin(\theta_1 + \theta_3 + \beta) \end{pmatrix} \tag{7}$$

$$\overrightarrow{P_4} = \begin{pmatrix} (r_0 + r_1) \cos\theta_1 + c_4 \cos(\theta_1 + \theta_4) \\ (r_0 + r_1) \sin\theta_1 + c_4 \sin(\theta_1 + \theta_4) \end{pmatrix} \tag{8}$$

$$R_1 = \theta_1 \tag{9}$$

$$R_2 = \theta_2 \tag{10}$$

$$R_3 = \theta_1 + \theta_3 \tag{11}$$

$$R_4 = \theta_1 + \theta_4 \tag{12}$$

where P_i is the position of each link's center of mass, R_i is the orientation of each link, r_i is the distance between two adjacent joints, c_i is the distance between the center of mass and the adjacent joint, and β is the angle between r_3 and c_3 (see Fig. 7).

There are kinematic constraints due to the four-bar mechanism that make the entire system have two degrees of freedom

$$r_1 + r_4 \cos\theta_3 = r_2 \cos\theta_2 + r_3 \cos\theta_4 \tag{13}$$

$$r_4 \sin\theta_3 = r_2 \sin\theta_2 + r_3 \sin\theta_4. \tag{14}$$

A Lagrange formulation was used to derive the equations of motion. Two generalized coordinates θ_1 and θ_2 were used to describe the equation. The kinetic energy of the system includes the translational and rotational kinetic energy of each link. The potential energy of the system includes the gravitational potential energy of each link, the elastic potential energy of the extensor spring, and the elastic potential energy of the flexor spring. As a result, two second-order nonlinear differential equations with respect to θ_1 and θ_2 were obtained. The equations of motion were solved numerically. The initial condition was chosen as

$$\theta_1 = \frac{\pi}{3} \tag{15}$$

$$\theta_2 - \theta_3 = \pi - \alpha - \varepsilon \tag{16}$$

where (15) is the angle between the tibia and ground, and (16) is the angle between the lower femur and coxa (see Fig. 7). α is the angle shown in Fig. 7. A negative ε makes the spring generate a counterclockwise latching torque, while a positive ε generates a clockwise extending torque. A small positive value of 2.86° (0.05 rad) was chosen for ε to simulate the state just after triggering. One of the solutions is shown in Fig. 9. The numerical solutions showed that θ_1 increases from an initial value, which means that the tibia rotates counterclockwise during the jump. θ_2 decreases from the initial value, which means that the lower femur rotates clockwise, which is the direction for the entire leg extension.

B. Takeoff

Takeoff occurs when the vertical reaction force on the ground reaches zero, after which, the foot detaches from the ground. The reaction force is determined by

$$m_{\mathrm{robot}} a_{\mathrm{robot},x} = \sum_{i=1}^{4} m_i a_{i,x}(t) = -H(t) \tag{17}$$

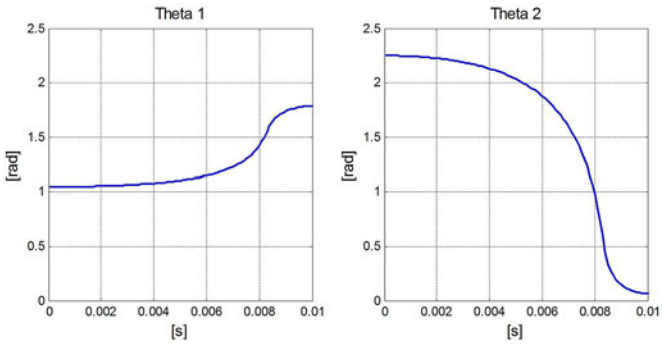

Fig. 9. Numerical solution ($r_1 = 5.5$ mm and $r_4 = 11$ mm).

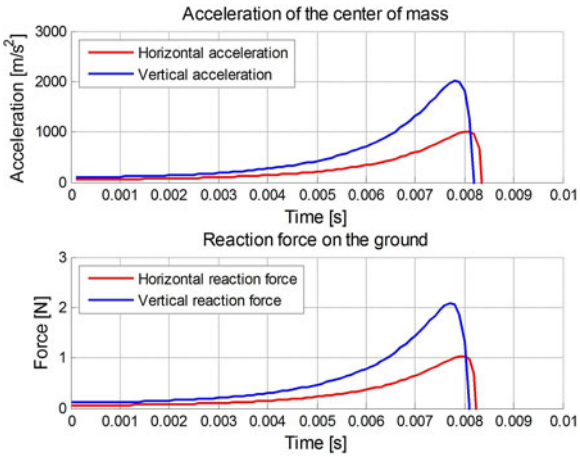

Fig. 10. Acceleration of the robot's center of mass and reaction force from the ground ($r_1 = 5.5$ mm and $r_4 = 11$ mm).

$$m_{\text{robot}} a_{\text{robot},y} = \sum_{i=1}^{4} m_i a_{i,y}(t) = V(t) - \sum_{i=1}^{4} m_i g \quad (18)$$

where m_{robot} is the total mass of the robot, a_{robot} is the acceleration of the robot's center of mass, a_i is the acceleration of each link, H is the horizontal reaction force on the ground, and V is the vertical reaction force on the ground.

The acceleration and reaction force profiles were obtained (see Fig. 10). When the vertical reaction force becomes zero, the robot takes off from the ground. The shapes of the acceleration and reaction force profiles are similar because gravitational acceleration is negligible compared with the large acceleration of the robot. This is the same phenomenon as the jumping of small creatures [30].

The acceleration of the robot's center of mass increases gradually and suddenly drops to zero, which is similar to that of an actual flea's acceleration [26]. This characteristic was derived from the mechanism of the flea-inspired catapult: As the femur rotates, the moment arm increases, thereby generating gradually increasing torque.

The robot's velocity at takeoff is determined by

$$m_{\text{robot}} v_{\text{robot}} = \sum_{i=1}^{4} m_i v_{i,f} \quad (19)$$

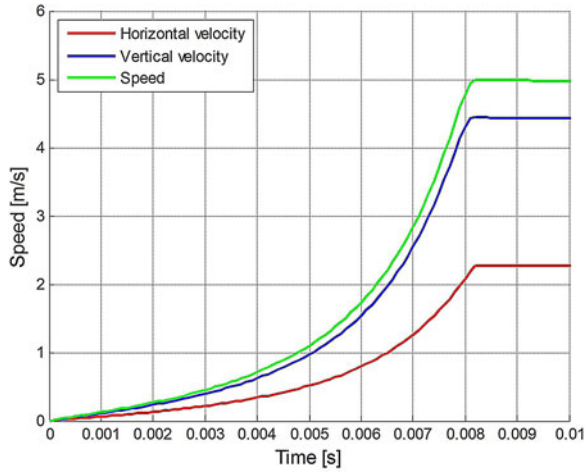

Fig. 11. Velocity of the robot's center of mass ($r_1 = 5.5$ mm and $r_4 = 11$ mm).

$$m_{\text{robot}} w_{\text{robot}} = \sum_{i=1}^{4} m_i w_{i,f} \quad (20)$$

where v_{robot} is the velocity of the robot's center of mass, and w_{robot} is the angular velocity of the robot. $v_{i,f}$ is the translational velocity, and $w_{i,f}$ is the angular velocity of each link just before takeoff.

The velocity profile of the robot's center of mass before and after takeoff was obtained (see Fig. 11). The speed of the robot's center of mass increases exponentially before takeoff and decreases slowly after takeoff due to gravitational acceleration.

C. Leg Optimization

The goal of leg optimization is to maximize the translational speed at takeoff by adjusting the leg length. r_1 and r_4 were chosen as the design variables. The design parameters chosen for optimization were r_1 and r_4 since they can effectively increase the speed at takeoff and are relatively easy to vary; modifying r_2 and r_3 could lead to modification of the entire coxa as well as rearrangement of the SMA springs.

The speed at takeoff was calculated with respect to various r_1 and r_4 (see Fig. 12). The ranges of r_1 and r_4 were 4–7 and 10–13 mm, respectively. There was a structural limit beyond which the latch of the robot could not operate: the dashed line in Fig. 12. If the robot's leg is designed to be on the upper side of the line, such as point (a), it cannot be latched even if the leg is fully flexed. The dashed line can be regarded as a boundary condition; thus, point (b) is the theoretical optimal point for the leg design.

However, points on the boundary condition, such as point (b), lack a sufficient margin for error, and the latch of the robot can be released inadvertently by a slight external disturbance. Considering the safety factor to make sure that the latch is stable, the actual prototype was fabricated using point (c), where r_1 is 5.5 mm and r_4 is 11 mm. The jumping speed at point (c) was 5.0 m/s, and the takeoff angle was 63°.

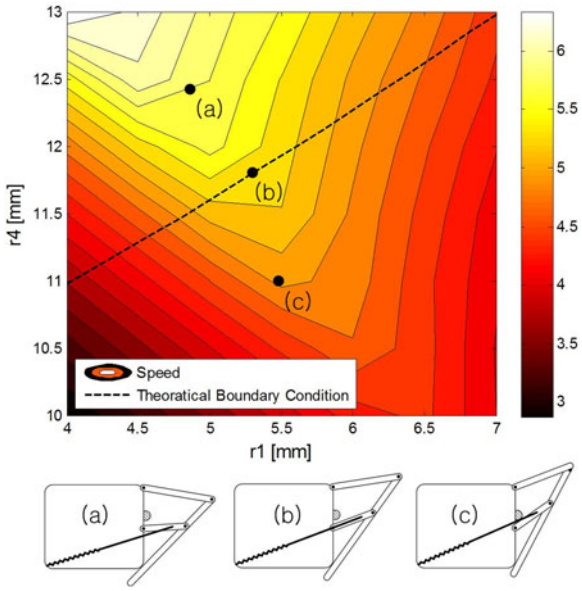

Fig. 12. Speed at takeoff with respect to various r_1 and r_4 values. In the region above the dashed line (e.g., point a), the latch of the robot cannot operate. On the dashed line (e.g., point b), the latch of the robot is unstable. The actual robot was fabricated at point c, considering the margin for a stable latch.

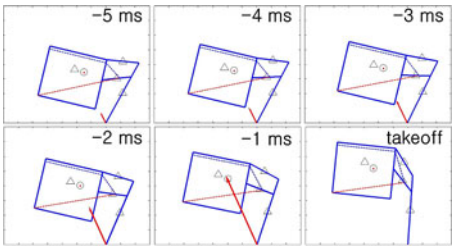

Fig. 13. Visualization of the jump ($r_1 = 5.5$ mm and $r_4 = 11$ mm)

According to the visualization of the jump (see Fig. 13), the design points on the ridgeline of the contour graph in Fig. 12, such as (a) and (b), allow robots to jump without rotation. In contrast, the robots rotate more as the design point moves away from the ridgeline. This means that the optimal leg design enables the robot to transform most of the stored energy to translational energy and little to rotational energy. The design points on the left side of the ridgeline generate clockwise rotation, whereas the points on the right side of the ridgeline generate counterclockwise rotation of the robots. Therefore, the actual robotic prototype fabricated using point (c) was anticipated to show clockwise rotation; this corresponded to the experimental results presented in Section VI.

The change in reaction force during jumping was also visualized to confirm the effect of the optimized leg from a dynamic point of view (see Fig. 13). The reaction force points toward the robot's center of mass during acceleration; therefore, the net impulse is applied precisely to the robot's center of mass. This reduces the redundant angular momentum and, thus, increases the translational momentum of the robot body.

In the visualization, the foot of the robot is detached from the ground before the leg is fully extended. Note that the upper

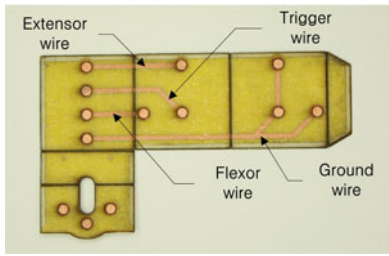

Fig. 14. Planar structure for the main body. Four electric wires are embedded: extensor, trigger, flexor, and ground wire.

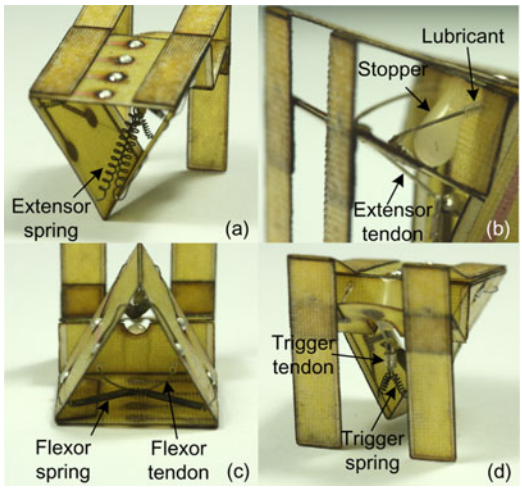

Fig. 15. Close views of the prototype. Each SMA spring is linked to each tendon and arranged in the body. Stopper and lubricant are attached to the body.

femur and the tibia are not in line at takeoff (see Fig. 13). This was because the extending speed of the leg was not able to catch up the releasing speed of the extensor due to the four-bar kinematic constraint. If a jumping robot prematurely leaves the ground before the spring fully recovers, part of the spring's stored energy will not be converted to useful kinetic energy [4].

V. Fabrication

The robot body was fabricated via the SCM process with embedded wiring [31]–[33]. For the main body, a planar structure was made by layering up sheets of glass fiber and copper-laminated Kapton (polyimide film). The copper layer on the Kapton had been etched to embed the electric wires in the main body (see Fig. 14). Planar structures for the legs are made through the same process but excluding the electric wiring. The planar structures for the main body and legs were cured in the vacuum stove first at 80 °C for 30 min and next at 140 °C for 60 min. The glass fiber segments then become rigid links and the film part exposed between each link function as flexure joints. The 3-D structure of the robot body is built by folding (see Fig. 15).

The extensor, flexor, and trigger were fabricated by coiling the SMA wire around a steel rod and annealing it at 300 °C for 1 h. Each spring was tailored according to the actuator design shown in Table II. The SMA actuators were arranged in the main body (see Fig. 15), and each tip was soldered to the copper

TABLE III
SPECIFICATION OF THE COMPONENTS

Components	Mass (g)	Portion (%)
Main body	0.542	49.1
Legs	0.248	22.5
Extensor Spring	0.035	3.2
Flexor Spring	0.025	2.3
Trigger Spring	0.01	1
Extensor Tendon	0.02	2
Flexor Tendon	0.02	2
Trigger Tendon	0.02	2
Solder	0.134	12.1
Adhesive	0.05	4.5
Total	1.104	100

terminal exposed on the main body as follows. First, a drop of flux (Indalloy Flux #2) is put on a glass plate, and the SMA is seared using a soldering iron, while both tips are immersed in the flux. Second, the stripped SMA is plated with a solder (96.5% Sn, 3% Ag, and 0.5% Cu). Finally, the SMA is soldered on the terminal.

The center of the extensor spring [see Fig. 15(a)] was linked to nylon-coated stainless steel wire, named extensor tendon [see Fig. 15(b)], whose tip was attached to the center of the femur. The center of the flexor spring [see Fig. 15(c)] was linked to another stainless steel wire, named flexor tendon [see Fig. 15(c)], whose tip was attached to the other side of the femur. Teflon tube lubricants [see Fig. 15(b)] were embedded in the main body to reduce friction on the flexor tendon. The trigger spring [see Fig. 15(d)] was linked to a trigger tendon [see Fig. 15(d)] and the tendon was hooked on an extensor tendon. The trigger tendon can slide on the extensor tendon so that the trigger spring would not exert parasitic tension after triggering. The tendons functioned not only as links but as insulators between SMA springs as well. A stopper [see Fig. 15(b)] was attached to the main body; it is the main element for the structural latch. The stopper constrains the femur to rotate over a certain angle, where the extensor tendon slightly passes the rotational center of the femur.

The robotic prototype was 1.1 g in weight, 20 mm in width, and 23 mm in height. Specification of the components is shown in Table III. There are three power terminals and one ground terminal on the body, which are connected to the external power supply unit through enameled wire.

VI. EXPERIMENTAL RESULTS

A. Jumping Performance

The jumping of the prototype was captured by a high-speed camera at 1500 frames/s (see Fig. 16). A ramp was used to adjust the angle between the tibia and ground to 60°, which was the same as the initial condition of the mathematical model. The prototype was powered by external power supply unit through enameled wires. When a current of 0.4 A was applied to the flexor for 4 s, the prototype flexed its leg and became poised to jump. Next, a 0.6-A current was applied to the extensor for 15 s. Enough time was set for this stage so that the flexor can cool down and does not impede the contraction of the extensor. There was no notable change in motion during this stage. Finally, 0.4 A of current was applied to the trigger for 2 s, and the robot jumped.

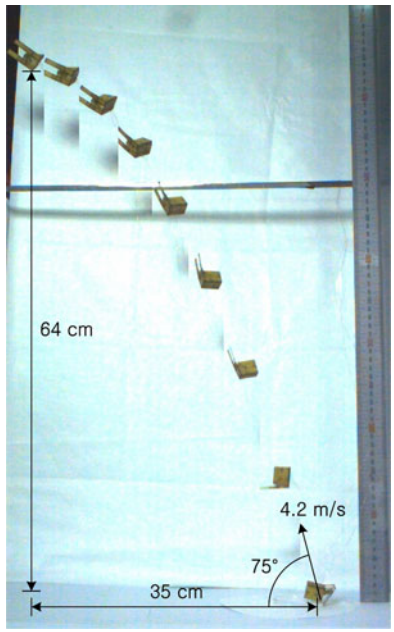

Fig. 16. Sequential pictures of the jumping motion (40-ms time intervals).

TABLE IV
EXTENSOR INPUT CURRENT VERSUS JUMPING HEIGHT

Input Current (A)	Spring Stiffness (N/mm)	Jumping Height (cm)
0.60	300	64
0.50	245	55
0.45	215	49
0.40	180	38

While the theoretical speed at takeoff was 5.0 m/s, the speed of the actual prototype was 4.2 m/s. The loss factors before takeoff may include joint friction, joint torsional stiffness, tendon frictions, and compliance of the tibia. While the theoretical takeoff angle was 63°, the takeoff angle of the actual prototype was 75°.

The jumping height of the current prototype was 64 cm at its peak, and the horizontal distance was 35 cm. This means that the current prototype can overcome obstacles approximately 30 times its body size. The trajectory of the current prototype is different from the ideal parabolic trajectory: 84-cm height and 45-cm distance at the peak. The loss factors include air drag and the load of the enameled wire, which is 0.15 g in weight.

The mechanical energy efficiency, which is the ratio of elastic energy stored to kinetic energy of the robot, was 26%. If we were to embed a 3.7-V Li-polymer battery (10 mAh), the total mass of the current prototype would increase to about 2 g (1.1 g for

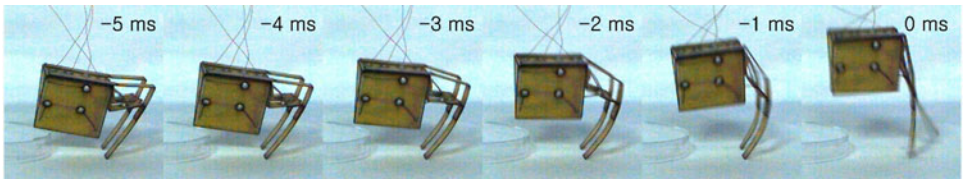

Fig. 17. Sequential pictures of the jumping motion (1-ms time intervals).

the current prototype, 0.4 g for battery, and about 0.5 g for additional circuitry).

As different amounts of current were applied to the extensor circuits (0.40–0.60 A), the jumping height was varied, as shown in Table IV. The amount of current input to the extensor spring determined the jumping speed as well as the jumping height and distance. This is the same as for an actual flea: Fleas, in general, vary the distance they jump by changing the jumping speed but not the jumping angle. This makes the amount of energy stored a crucial control parameter of the flea's jump [26].

Compared with a previous study [34], where the prototype jumped 7.5 times its body size, the current prototype showed an improved performance. Factors for the improvement include 1) deriving a new dynamic modeling applicable to general four-bar legs; 2) optimizing the leg design to increase the speed at takeoff; 3) designing SMA actuators based on experimental results; and 4) modifying the body design to resolve previous problems, such as fatigue failure of the copper wire, friction on a tendon, and providing insulation for SMA springs.

B. Motion Before Takeoff

The jumping of the prototype was captured by a high-speed camera at 3000 frames/s (see Fig. 17) to observe the motion before takeoff in detail. Although not considered in the mathematical model, an unintentional spring effect of the compliant leg was observed; the tibia was gradually bent and restraightened during acceleration. Due to the bending of the tibia, the body slightly shifts backward before jumping, which explains why the jumping angle has increased from 63° to 75°.

The velocity profile was obtained by plotting the average velocity every 1 ms (see Fig. 18). The reaction force profile was obtained from the average acceleration every 1 ms (see Fig. 19). Both mathematical and experimental profiles were shifted to set the takeoff time to zero. While the experimental velocity profile seemed to match well with the theoretical result, the experimental reaction force showed discrepancy from the theoretical result: The reaction force of the mathematical model increases exponentially and reaches a sharp peak just before takeoff, but the actual reaction force showed a more reduced peak. The flattened force profile is because of the compliant tibia that functions like a suspension; the stiffness of the tibia is comparable with that of the extensor spring. The reduced peak of the reaction force is advantageous for miniature jumping robots because it prevents structural failure and slippage problems [8].

While the model showed premature jumping in Section IV, this phenomenon disappeared in the actual prototype. Note that

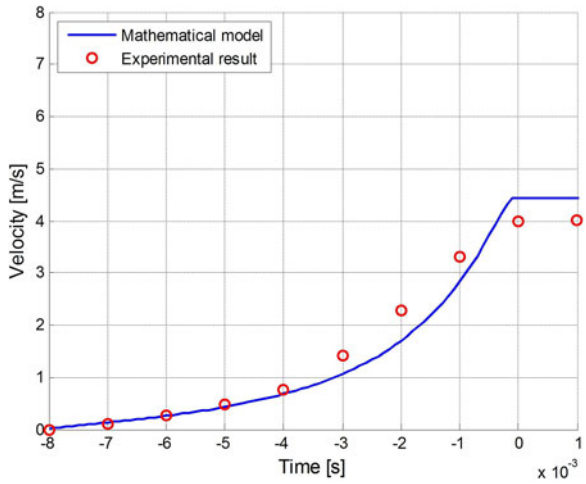

Fig. 18. Vertical velocity profile during takeoff. Both profiles of the mathematical model and actual robot were shifted to set the time at takeoff to zero.

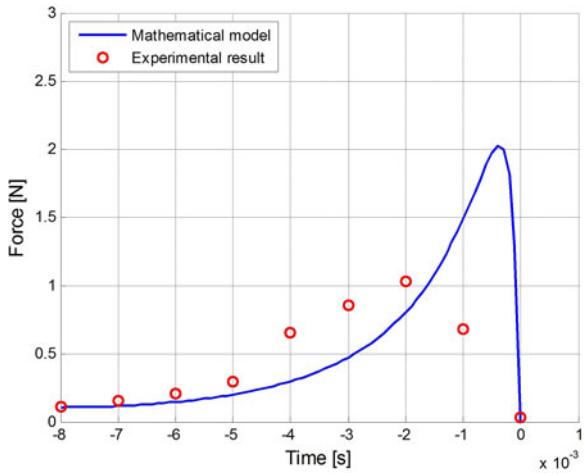

Fig. 19. Vertical reaction force profiles of the mathematical model and actual robot. The profile of the actual robot was shifted to set the time at takeoff to zero.

the upper femur and the tibia of the actual prototype are in line at takeoff (see Fig. 17). As opposed to the model made up of a rigid four-bar link, the actual prototype has compliance in the tibia. The compliant tibia provides an additional degree of freedom, which enables the prototype to present a modified four-bar link motion. This may explain why premature jumping disappeared in the actual prototype.

A detailed quantitative study of the effect of the compliant tibia on the jumping performance would enable optimization of the compliance to further improve the jumping performance.

VII. Conclusion

In this paper, we have presented a novel flea-inspired catapult mechanism for miniature jumping robots. A robotic design is proposed to realize the mechanism of the biological catapult by taking advantage of the characteristics of SMA spring actuators. SMA spring actuators replace conventional actuators, transmissions, and elastic element to help reduce the size. The SCM enables the body design to be compact and lightweight, while providing a rigid frame for attaching the actuators. A four-bar mechanism was designed using SCM to generate an effective jumping motion. Modeling enabled us to design the leg such that the net thrust force passes through the center of mass, eliminating body rotation during the jump. It also allowed us to design the leg so as to maximize the speed at takeoff, while keeping it within the structural limit. To demonstrate the feasibility of the mechanism, a robotic prototype weighing 1.1 g and having a body size of 2 cm was fabricated; the prototype can jump up to 30 times its body size. The measured velocity profile generally matched with that derived from the model, although the measured acceleration profile changed favorably from that of the model. The compliance of the leg may be the reason behind this change.

Although the prototype was used to successfully realize the flea-inspired catapult mechanism, a few more components are needed to build an autonomous jumping robot using this mechanism. First, the power supply unit and control electronics need to be onboard, which is a challenge due to the light weight of the robot itself. Second, a mechanism for the robot to stably land and stay upright needs to be developed. Third, a mechanism to adjust the takeoff angle needs to be installed.

There is no guarantee that the biological principle of a flea's jump is the optimal solution for a microjumping robot. From a mechanical point of view, however, the mechanism is attractive since it can handle large elastic energy easily and may enable the miniaturization of jumping robots due to its scalable design.

References

[1] M. Kaspari and M. D. Weiser, "The size-grain hypothesis and interspecific scaling in ants," *Funct. Ecol.*, vol. 13, no. 4, pp. 530–538, 1999.

[2] R. J. Wood, "The first takeoff of a biologically inspired at-scale robotic insect," *IEEE Trans. Robot.*, vol. 24, no. 2, pp. 341–347, Apr. 2008.

[3] W. Gronenberg, "Fast actions in small animals: Springs and click mechanisms," *J. Comp. Physiol. A: Sens., Neural, Behav. Physiol.*, vol. 178, no. 6, pp. 727–734, 1996.

[4] P. Fiorini and J. Burdick, "The development of hopping capabilities for small robots," *Auton. Robots*, vol. 14, no. 2–3, pp. 239–254, 2003.

[5] B. G. A. Lambrecht, A. D. Horchler, and R. D. Quinn, "A small, insect-inspired robot that runs and jumps," in *Proc. IEEE Int. Conf. Robot. Autom.*, Apr., 2005, pp. 1240–1245.

[6] R. Armour, K. Paskins, A. Bowyer, J. Vincent, and W. Megill, "Jumping robots: A biomimetic solution to locomotion across rough terrain," *Bioinspiration Biomimetics*, vol. 2, no. 3, pp. S65–S82, 2007.

[7] U. Scarfogliero, C. Stefanini, and P. Dario, "Design and development of the long-jumping 'Grillo' mini robot," in *Proc. IEEE Int. Conf. Robot. Autom.*, Apr. 2007, pp. 467–472.

[8] F. Li, G. Bonsignori, U. Scarfogliero, D. Chen, C. Stefanini, W. Liu, P. Dario, and X. Fu, "Jumping mini-robot with bio-inspired legs," in *Proc. IEEE Int. Conf. Robot. Biomimetics*, Feb. 2008, pp. 933–938.

[9] U. Scarfogliero, C. Stefanini, and P. Dario, "The use of compliant joints and elastic energy storage in bio-inspired legged robots," *Mech. Mach. Theory*, vol. 44, no. 3, pp. 580–590, 2009.

[10] M. Kovač, M. Fuchs, A. Guignard, J.-C. Zufferey, and D. Floreano, "A miniature 7 g jumping robot," in *Proc. IEEE Int. Conf. Robot. Autom.*, 2008, pp. 373–378.

[11] M. Kovač, M. Schlegel, J.-C. Zufferey, and D. Floreano, "A miniature jumping robot with self-recovery capabilities," in *Proc. IEEE/RSJ Int. Conf. Intell. Robots Syst.*, Oct., 2009, pp. 583–588.

[12] M. Kovač, M. Schlegel, J.-C. Zufferey, and D. Floreano, "Steerable miniature jumping robot," *Auton. Robots*, vol. 28, no. 3, pp. 295–306, 2010.

[13] A. Yamada, M. Watari, H. Mochiyama, and H. Fujimoto, "A jumping robot based on the closed elastica," in *Proc. Int. Symp. Micro-NanoMechatron. Human Sci.*, 2007, pp. 604–609.

[14] A. Yamada, M. Watari, H. Mochiyama, and H. Fujimoto, "An asymmetric robotic catapult based on the closed elastica for jumping robot," in *Proc. IEEE Int. Conf. Robot. Autom.*, May 2008, pp. 232–237.

[15] P. Zhang and Q. Zhou, "Voice coil based hopping mechanism for microrobot," in *Proc. IEEE Int. Conf. Robot. Autom.*, May 2009, pp. 3001–3006.

[16] S. Dubowsky, S. Kesner, J.-S. Plante, and P. Boston, "Hopping mobility concept for search and rescue robots," *Int. J. Ind. Robot*, vol. 35, no. 3, pp. 238–245, 2008.

[17] W. Churaman, L. Currano, C. Morris, J. Rajkowski, and S. Bergbreiter, "The first launch of an autonomous thrust-driven microrobot using nanoporous energetic silicon," *IEEE/ASME J. Microelectromechanical Syst.*, vol. 21, no. 1, pp. 198–205, Feb. 2012.

[18] A. P. Gerratt, I. Penskiy, and S. Bergbreiter, "Integrated silicon-PDMS process for microrobot mechanisms," in *Proc. IEEE Int. Conf. Robot. Autom.*, May 2010, pp. 3153–3158.

[19] W. A. Churaman, A. P. Gerratt, and S. Bergbreiter, "First leaps toward jumping microrobots," in *Proc. IEEE/RSJ Int. Conf. Intell. Robots Syst.*, Sep. 2011, pp. 1680–1686.

[20] H. C. Bennet-Clark and E. C. Lucey, "The jump of the flea: A study of the energetics and a model of the mechanism," *J. Exp. Biol.*, vol. 47, no. 1, pp. 59–67, 1967.

[21] R. J. Wood, S. Avadhanula, R. Sahai, E. Steltz, and R. S. Fearing, "Microrobot design using fiber reinforced composites," *J. Mech. Des.*, vol. 130, no. 5, pp. 052304–052311, 2008.

[22] W. F. Lyon, "Fleas (HYG-2081-97)," *Ohio State University Extension Fact Sheet: Entomology,* Columbus, OH, 1991.

[23] M. Rothschild and J. Schlein, "The jumping mechanism of Xenopsylla cheopis. I. Exoskeletal structures and musculature," *Philos. Trans. Roy. Soc. Lond. B, Biol. Sci.*, vol. 271, no. 914, pp. 457–490, 1975.

[24] M. J. Cullen, "The jumping mechanism of Xenopsylla cheopis. II. The fine structure of the jumping muscle," *Philos. Trans. Roy. Soc. Lond. B, Biol. Sci.*, vol. 271, no. 914, pp. 491–497, 1975.

[25] M. Rothschild, J. Schlein, K. Parker, C. Neville, and S. Sternberg, "The jumping mechanism of Xenopsylla cheopis. III. Execution of the jump and activity," *Philos. Trans. Roy. Soc. Lond. B, Biol. Sci.*, vol. 271, no. 914, pp. 499–515, 1975.

[26] G. P. Sutton and M. Burrows, "Biomechanics of jumping in the flea," *J. Exp. Biol.*, vol. 214, no. 5, pp. 836–847, 2011.

[27] K. Otsuka and C. M. Wayman, *Shape Memory Materials*. Cambridge, U.K.: Cambridge Univ. Press, 1998, pp. 240–266.

[28] S. Kim, E. Hawkes, K. Choy, M. Joldaz, J. Foleyz, and R. Wood, "Micro artificial muscle fiber using NiTi spring for soft robotics," in *Proc. IEEE/RSJ Int. Conf. Intell. Robots Syst.*, Oct. 2009, pp. 2228–2234.

[29] L. L. Howell, *Compliant Mechanisms*. New York: Wiley-Interscience, 2001, pp. 136–140.

[30] M. Scholz, M. Bobbert, and A. K. van Soest, "Scaling and jumping: Gravity loses grip on small jumpers," *J. Theor. Biol.*, vol. 240, pp. 554–561, 2006.

[31] K.-J. Cho, E. Hawkes, C. Quinn, and R. J. Wood, "Design, fabrication and analysis of a body-caudal fin propulsion system for a microrobotic fish," in *Proc. IEEE Int. Conf. Robot. Autom.*, May 2008, pp. 706–711.

[32] J.-S. Koh and K.-J. Cho, "Omegabot: Biomimetic inchworm robot using SMA coil actuator and smart composite microstructures (SCM)," in *Proc. IEEE Int. Conf. Robot. Biomimetics*, Dec. 2009, pp. 1154–1159.

[33] J. -S. Koh, S. -M. An, and K. -J. Cho, "Finger-sized climbing robot using artificial proleg," in *Proc. IEEE/RAS Int. Conf. Biomed. Robot. Biomechatron.*, Sep. 2010, pp. 610–615.

[34] M. Noh, S. Kim, and K.-J. Cho, "A miniature jumping robot with flea-inspired catapult system: Active latch and trigger," in *Proc. Int. Workshop on Bio-Inspired Robots*, 2011. [Online]. Available: http://www.emn.fr/z-dre/bionic-robots-workshop/index.php?page=poster-session.

Minkyun Noh received the B.S. degree in mechanical and aerospace engineering from Seoul National University, Seoul, Korea, in 2012.

From 2008 to 2010, he performed military duty as an Assistant Instructor for an engineering equipment maintenance course with the Army Engineer School, Jangseong, Korea. He is currently a Research Assistant with the Biorobotics Laboratory, Seoul National University. His current research interests include bioinspired robot design, smart actuators, and applications of compliant material.

Seung-Won Kim (S'10) received the B.S. degree in mechanical and aerospace engineering from Seoul National University, Seoul, Korea, in 2009, where he is currently working toward the Ph.D. degree in mechanical engineering with the Biorobotics Laboratory.

His current research interests include the conception, design, and fabrication of bioinspired robots, particularly small-scale mobile and soft morphing robots, as well as smart actuators and bistable composite structures.

Mr. Kim received the Best Paper Award in Robotics from the Korean Society for Precision Engineering in Spring 2010 and won the Best Student Paper Award from the IEEE Robotics and Automation Society/Engineering in Medicine and Biology Society International Conference on Biomedical Robotics and Biomechatronics in 2010.

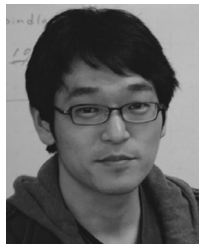

Sungmin An received the B.S. degree in mechanical engineering from Yonsei University, Seoul, Korea, in 2009 and the M.S. degree from Seoul National University in 2011.

He is currently a Researcher with the Biorobotics Laboratory, Seoul National University. His current research interests include the design and characterization of smart actuators and biomimetic robotics.

Je-Sung Koh (S'10) received the B.S. degree in mechanical and aerospace engineering from Seoul National University, Seoul, Korea, in 2008, where he is currently working toward the Ph.D. degree with the Biorobotics Laboratory.

His current research interests include bioinspired robot design and small-scale robot design with smart materials.

Mr. Koh received the Best Student Paper Award from the IEEE/Robotic Society of Japan at the Engineering in Medicine and Biology Society International Conference on Biomedical Robotics and Biomechatronics in 2010.

Kyu-Jin Cho (M'08) received the B.S. and M.S. degrees from Seoul National University, Seoul, Korea, in 1998 and 2000, respectively, and the Ph.D. degree in mechanical engineering from the Massachusetts Institute of Technology, Cambridge, in 2007.

He was a Postdoctoral Fellow with Harvard Microrobotics Laboratory until 2008. He is currently an Assistant Professor of mechanical and aerospace engineering and the Director of Biorobotics Laboratory, Seoul National University. His research interests include biologically inspired robotics, robotics systems using smart actuators, novel mechanisms using smart structures, and rehabilitation and assistive robotics.